Hindawi
Journal of Chemistry
Volume 2019, Article ID 8620181, 10 pages
https://doi.org/10.1155/2019/8620181

Research Article

Fabrication of Porous Hydroxyapatite Granules as an Effective Adsorbent for the Removal of Aqueous Pb(II) Ions

Duyen Thi Le,[1,2] **Thao Phuong Thi Le**,[1] **Hai Thi Do**,[1] **Hanh Thi Vo**,[1,3] **Nam Thi Pham**,[3] **Thom Thi Nguyen**,[3] **Hong Thi Cao**,[3] **Phuong Thu Nguyen**,[3] **Thanh Mai Thi Dinh**,[4,5] **Hai Viet Le**,[6,7] **and Dai Lam Tran**[3,5]

[1]*Department of Chemistry, Basic Science Faculty, Hanoi University of Mining and Geology, 18 Pho Vien, Duc Thang, Bac Tu Liem, Hanoi, Vietnam*
[2]*Center for Excellence in Analysis and Experiment, Hanoi University of Mining and Geology, 18 Pho Vien, Duc Thang, Bac Tu Liem, Hanoi, Vietnam*
[3]*Institute for Tropical Technology, Vietnam Academy of Science and Technology, 18 Hoang Quoc Viet, Cau Giay, Hanoi, Vietnam*
[4]*University of Science and Technology of Hanoi, Vietnam Academy of Science and Technology, 18 Hoang Quoc Viet, Cau Giay, Hanoi, Vietnam*
[5]*Graduate University of Science and Technology, Vietnam Academy of Science and Technology, 18 Hoang Quoc Viet, Cau Giay, Hanoi, Vietnam*
[6]*Laboratory of Advanced Materials Chemistry, Advanced Institute of Materials Science, Ton Duc Thang University, Ho Chi Minh City, Vietnam*
[7]*Faculty of Applied Sciences, Ton Duc Thang University, Ho Chi Minh City, Vietnam*

Correspondence should be addressed to Duyen Thi Le; lethiduyen@humg.edu.vn and Dai Lam Tran; trandailam@gmail.com

Received 15 August 2018; Revised 5 January 2019; Accepted 22 January 2019; Published 21 February 2019

Academic Editor: Yingchao Dong

Porous hydroxyapatite (HAp) granules have been successfully fabricated from a HAp powder precursor and polyvinyl alcohol (PVA) additive by a simple sintering process. The composition and microstructures of the HAp were characterized by X-ray diffraction (XRD) and scanning electron microscope (SEM) equipped with an energy dispersive X-ray (EDX) spectrometer. The effects of sintering temperature and PVA/HAp mass ratios on color, water stability, morphology, and chemical composition of HAp are discussed. Optimum conditions for the fabrication of HAp granules were found to be a PVA/HAp mass ratio of 3/20 and a sintering temperature of 600°C for 4 h. Accordingly, the obtained HAp is white in color, is in the granular form with a size of about 2×10 mm, and has a specific surface area of 70.6 m^2/g. The adsorption of Pb^{2+} onto the as-prepared HAp granules was carried out in aqueous solution by varying the pH, the adsorbent dose, the initial concentration of Pb^{2+}, and the contact time. The results of adsorption stoichiometry of Pb^{2+} on the HAp granule adsorbent were fitted to the Langmuir adsorption isotherm model ($R^2 = 0.99$). The adsorption capacity and removal efficiency of the HAp granule adsorbent for Pb^{2+} under optimal conditions were found to be 7.99 mg/g and 95.92%, respectively. The adsorption process obeyed a pseudo-second-order kinetic model with $R^2 \sim 1$. The porous HAp granules studied in this work showed potential for the removal of Pb^{2+} from industrial wastewater.

1. Introduction

Nowadays, pollution of the water environment caused by heavy metals, mainly from industrial waste, becomes one of the most serious problems. Various methods of removing heavy metal ions have been widely studied, such as chemical precipitation, electrochemical deposition, membrane filtration, ion exchange, adsorption, biological treatment, and stabilization/solidification [1–6]. Among these methods, the adsorption method gives high efficiency for treatment, so it has been used widely. In recent years, many porous materials have been used for the adsorption of heavy metals in aqueous

solution, such as activated carbon, clays, zeolites, apatite, chitosan, bioadsorbents, and agricultural wastes [1, 7]. In general, studies on materials which have high removal efficiency, are of low cost, and are nontoxic to human health are essential. In this regard, several normal adsorbents have been recommended to remove Pb^{2+} ions. More recently, calcium hydroxyapatite ($Ca_{10}(PO_4)_6(OH)_2$, noted as HAp) is of interest to many researchers because of its remarkable adsorption efficiency for long-term containment.

Synthetic HAp has a similar chemical composition to the inorganic matrix of the natural bone and has good biological activity [8]. It has therefore been applied in the field of medicine and pharmacy [9–11]. HAp is nontoxic and nonallergic to humans and has antibacterial properties [8]. In addition to the biomedical field, HAp has been applied in the treatment of the environment. HAp can eliminate several contaminants such as Cu^{2+}, Pb^{2+}, Zn^{2+}, Cd^{2+}, Co^{2+}, and Ni^{2+} [12–18] as well as NO_3^-, PO_4^{3-}, F^-, phenol, nitrobenzene, and red congo [19–24] of aqueous solutions. In addition, it has been used in chromatography for fractionation and purification of proteins and nucleic acids [25]. Depending on the applicable purpose, HAp is prepared in various forms, including powder, membrane, composite, and ceramic by physical, chemical, and electrochemical methods. The HAp ceramics have been fabricated with or without additives according to many methods, such as freeze casting [26], sintering [27, 28], ice templating [29], direct foaming [30], or polymeric sponge [31] for application in the biomedical industry. Some pore-forming additives have been used to make porous HAp ceramics, such as carbonate salt, hydrogen peroxide, carbon, starch, flour [32], paraffin, naphthalene, polyvinyl butyral [32, 33], and polyvinyl alcohol (PVA) [26, 29]. In addition, several reports on the fabrication of HAp granules have been applied for treatment of the environment [34, 35]. However, very few reports deal with the fabrication of HAp granules with PVA additive as an effective adsorbent for the removal of Pb(II) ions in aqueous solutions. Herein, we describe the fabrication of HAp granules by the sintering method and its application as an adsorbent for removal of Pb^{2+} ions from an aqueous solution. The influence of parameters such as adsorbent dose, contact time, and initial concentration of Pb^{2+} was investigated. The adsorption process has been studied via isotherms and kinetics.

2. Materials and Methods

2.1. Materials. $Ca(NO_3)_2{\cdot}4H_2O$ 98%, $(NH_4)_2HPO_4$ 99%, NH_3 25–28%, $Pb(NO_3)_2$ 99%, polyvinylalcohol (PVA), KNO_3 99%, KOH 99%, and HNO_3 65% are pure chemicals and are ordered from Merck.

2.2. Preparation of HAp Powder. HAp powder is prepared by a wet chemical precipitation method from $Ca(NO_3)_2{\cdot}4H_2O$ and $(NH_4)_2HPO_4$ salts in water following reaction (1) [36]. Accordingly, the aqueous solution of 0.3 M $(NH_4)_2HPO_4$ is slowly added dropwise into a 0.5 M solution of $Ca(NO_3)_2$ at a rate of 1 mL·min^{-1}. During the process, the pH value of the solution is adjusted to about 10 using the concentrated NH_3 solution. The reaction is carried out at 25°C with continuous stirring (800 rpm). The obtained precipitate is aged for 15 h and then repeatedly centrifuge-washed with distilled water until neutral pH and then dried at 80°C in 24 h. The obtained HAp powder is white with a size less than 100 nm [36]:

$$10\mathrm{Ca}(\mathrm{NO_3})_2 + 6(\mathrm{NH_4})_2\mathrm{HPO_4} + 8\,\mathrm{NH_3} + 2\,\mathrm{H_2O} \longrightarrow \mathrm{Ca_{10}(PO_4)_6(OH)_2} + 20\,\mathrm{NH_4NO_3} \quad (1)$$

2.3. Fabrication of HAp Granules. The porous HAp granules are fabricated by the sintering method from HAp powder and PVA additive (with different PVA/HAp mass ratios of 2/20, 3/20, 4/20, and 5/20 denoted H_2, H_3, H_4, and H_5, respectively) at calcining temperatures: 400, 600, and 700°C. The sintering time for each experiment is 4 h.

The phase component of HAp powder and granules is analyzed by X-ray diffraction (XRD) using a Siemens D5000 diffractometer, CuK_α radiation ($\lambda = 1.54056$ Å) with a step angle of 0.030°, the scanning rate of 0.04285° s^{-1}, and 2θ degree in a range of 5–70°. The surface morphology of HAp granules is examined using a Hitachi S-4800 scanning electron microscope (SEM). The composition of elements in HAp granules is identified using JSM 6490-JED 1300 Jeol (Japan) energy-dispersive X-ray spectroscopy (EDX). The specific surface area of HAp granules is determined from low-temperature nitrogen adsorption isotherms following the Brunauer, Emmett, and Teller (BET) method, using a Micrometrics ASAP 2000 instrument. The thermal stability of HAp powder and PVA is examined by the thermogravimetric analysis (TGA) method using TGA209 F1 NETZSCH.

2.4. Determination of pH_{PZC}. A mixture of 0.30000 g of HAp granules in 50.0 mL of 0.01 M KNO_3 solution is shaken for 60 minutes at room temperature. The initial pH values (pH_0) are adjusted in the range of 2.5–9.5 using 0.1 M KOH or 0.1 M HNO_3 solution. After equilibration, the pH values are measured once again (pH_f), and the value of pH_{PZC} (point of zero charge) is determined from the $\Delta pH = f(pH_0)$ plot ($\Delta pH = pH_0 - pH_f$). pH_{PZC} is the pH_0 value when $\Delta pH = 0$ [37].

2.5. Adsorption Experiments. The experiments are carried out by mixing a quantity of HAp granules with 50 mL of Pb^{2+} ion solution. The effect of physicochemical parameters on the adsorption process is investigated: the initial concentration of Pb^{2+} solution varies between 5 and 100 mg/L, the contact time varies between 5 and 60 min, the initial pH of the solution is studied between 2.5 and 7.5, and the dose of HAp granules is in the range of 2–26 g/L. The experiments are carried out at room temperature and with continuous shaking using a mechanical shaker at 100 rpm. After filtration to remove the solid, the remaining concentration of Pb^{2+} is determined by using an atomic absorption spectrophotometer (AAS).

The adsorption capacity and the removal efficiency are calculated by using equations (2) and (3), respectively [13]:

$$Q = (C_0 - C) \cdot \frac{V}{m}, \tag{2}$$

$$H = (C_0 - C) \cdot \frac{100}{C_0}, \tag{3}$$

where Q represents the adsorption capacity of Pb^{2+} at equilibrium (mg/g), H represents the removal efficiency of Pb^{2+}(%), C_0 and C are the initial and equilibrium concentrations (mg/L) of Pb^{2+} in solution, respectively, and V and m are the solution volumes (L) and the mass of HAp granules (g), respectively.

The obtained experimental data are analyzed using the Langmuir and Freundlich isotherm models [13, 14]:

$$\text{Langmuir linear equation: } \frac{C_e}{Q} = \frac{C_e}{Q_m} + \frac{1}{K_L \cdot Q_m},$$
$$\text{Freundlich linear equation: } \ln Q = \ln K_F + \frac{1}{n} \ln C_e, \tag{4}$$

where C_e (mg/L) is the equilibrium concentration of Pb^{2+}, Q (mg/g) is the amount adsorbed at equilibrium, Q_m (mg/g) is the maximum adsorption capacity, K_L is the Langmuir coefficient related to the adsorption energy, and K_F and n are the constants of the Freundlich model.

The adsorption kinetics is described by the pseudo-first-order and pseudo-second-order kinetic models using equations (5) and (6), respectively [13]:

$$\ln (Q_e - Q_t) = \ln Q_e - k_1 t, \tag{5}$$

$$\frac{t}{Q_t} = \frac{t}{Q_e} + \frac{1}{(k_2 \cdot Q_e^2)}, \tag{6}$$

where Q_e is the adsorption capacity at equilibrium (mg/g), Q_t is the adsorption capacity at time t (mg/g), and k_1 and k_2 are pseudo-first-order (min^{-1}) and pseudo-second-order (g/mg/min) rate constants, respectively.

3. Results and Discussion

3.1. Fabrication of HAp Granules

3.1.1. Thermal Stability of HAp Powder and Polyvinyl Alcohol (PVA). The weight loss of HAp powder is measured in the temperature range of 30 to 1000°C by the thermogravimetric analysis method. As shown in Figure 1(a), the mass of the sample decreases 5.55% at about 200°C, which corresponds to the loss of water adsorbed in HAp powder. When increasing the temperature up to about 1000°C, no peak appeared, but the sample mass decreases further by 4.28%, which corresponds to the process of structural water loss in HAp. This result is assumed to be the progressive dehydroxylation of HAp, as shown in the following equation [38]:

$$Ca_{10}(PO_4)_6(OH)_2 \longrightarrow Ca_{10}(PO_4)_6(OH)_{2-2x}O_x + xH_2O \tag{7}$$

The XRD patterns of HAp samples prepared at different sintering temperatures are shown in Figure 2. At the sintering temperature of 700°C and 850°C, there is only one phase of HAp in the samples. When the sintering temperature is increased to about 1000°C, the XRD pattern showed a new $Ca_3(PO_4)_2$ phase in the sample. The HAp granules can therefore be fabricated from HAp powder at a sintering temperature of less than 1000°C.

Typically, the melting temperature of PVA is determined indirectly at about 200°C. When the PVA is heated under vacuum at 200°C, it decomposes into water and brown powder. Continuing with the heat of PVA at 400°C, it breaks down into volatile hydrocarbon molecules and nonvolatile products. The result of the thermogravimetric analysis is shown in Figure 1(b). At 250°C, the mass of the sample decreases by 4.07% and, up to about 600°C, the mass of the sample decreases by more than 95.71%, which corresponds to the complete decomposition of PVA. Therefore, the HAp granules can be fabricated from HAp powder with PVA additive and sintered at a temperature of 600°C or higher.

3.1.2. Effect of PVA/HAp Mass Ratio. To study the effect of the amount of PVA additive on the color, the durability in water, and the physicochemical characteristics of the obtained material, the HAp granules with different PVA/HAp mass ratios of 2/20 (H_2), 3/20 (H_3), 4/20 (H_4), and 5/20 (H_5) are fabricated. After that, the samples are sintered at 600°C for 4 h.

The result shows that, at 600°C and 4 h sintering, samples H_2 and H_3 are white, while H_4 and H_5 are still grey. This result can be explained by the fact that, with a higher mass ratio of PVA/HAp (4/20, 5/20), the sintering time of 4 h is not sufficient to completely decompose the PVA in the samples. However, increasing of the sintering time is not a benefit of the energy. Therefore, H_4 and H_5 granule samples will not be fabricated. The physicochemical characteristics of obtained H_2 and H_3 granules including the durability in water, specific surface area, and morphology are presented in Table 1 and Figure 3.

Both H_2 and H_3 samples have a relatively uniform surface, while the H_3 sample shows lower disintegration in water and a larger specific surface area than H_2, so its adsorption capacity is higher. This is because the increase of the PVA content leading to the binding in the material structure is better and the porous enhancements lead to an increase in the specific surface area. Therefore, the H3 granules are chosen for further studies.

3.1.3. Effect of Sintering Temperature. As the sintering temperature increases, the mass percentage of HAp disintegration decreases. This means that the durability in water of granules increases after 4 h and 8 h shaking (Table 2). This is in agreement with the fact that, by increasing the sintering temperature, the adhesiveness of

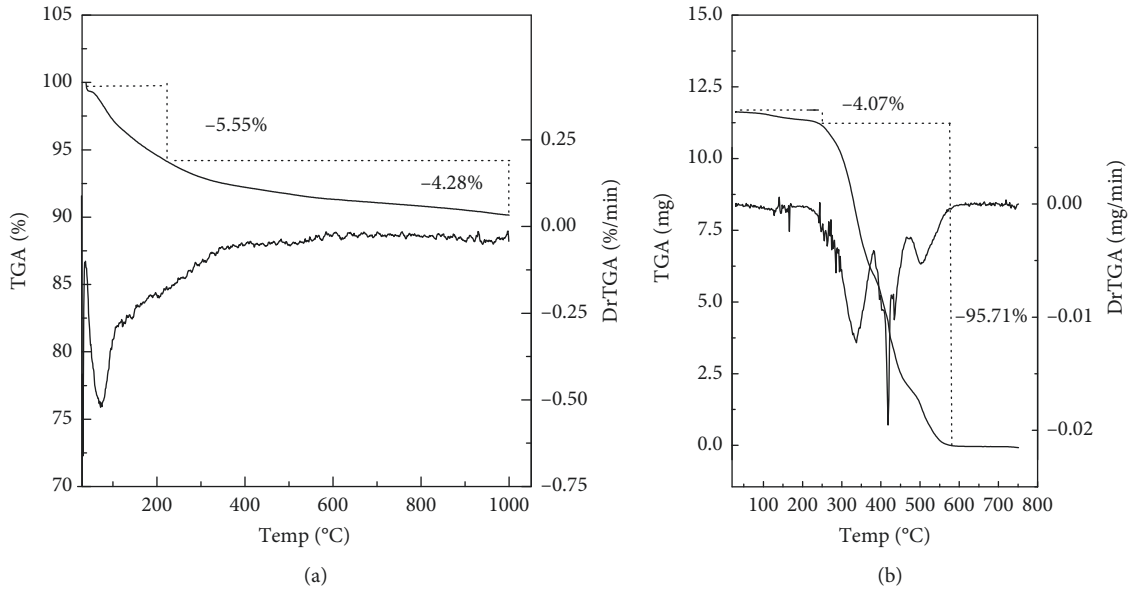

Figure 1: TGA curves of (a) HAp powder and (b) PVA.

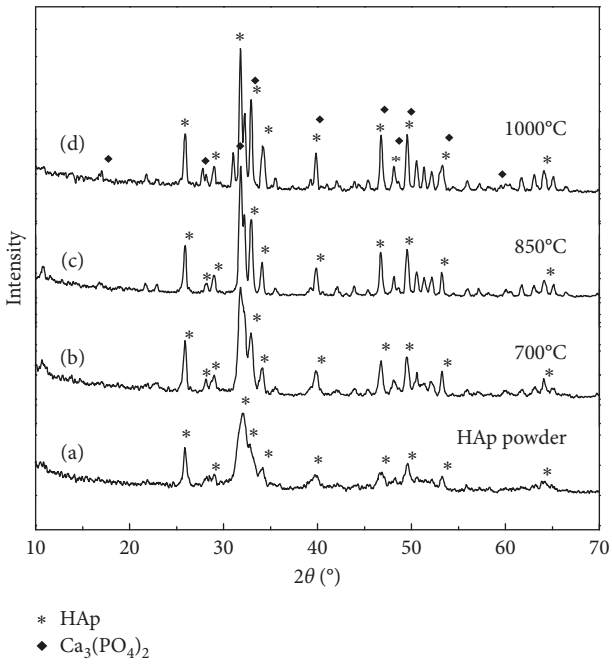

Figure 2: XRD patterns of (a) HAp powder, after sintering at (b) 700°C, (c) 850°C, and (d) 1000°C.

the material increases and the structure of the granules is closely bonded, resulting that disintegration in water decreases.

Sample H_3 sintered at 400°C for 4 h is black because this temperature is not high enough to completely decompose the PVA in the sample. Accordingly, the disintegration in water is high, and the granules cannot be fabricated under this condition. H_3 samples sintered at 600°C and 700°C for 4 h are white in color and are used for further study of the physicochemical characteristics.

Table 1: The color, durability in water, and specific surface area of HAp granules sintered at 600°C for 4 h.

Sample	Color	% mass of HAp disintegration in water		S_{BET} (m^2/g)
		4 h	8 h	
H_2	White	15.4	26.5	67.6
H_3	White	10	20	70.6
H_4	Grey			
H_5	Grey			

The XRD results show that H_3 granules sintered at 600°C and 700°C are a single phase of HAp (Figure 4). The Ca/P and Ca/P/O ratios in HAp granules (EDX data) at 600°C (Ca/P = 1.646; Ca/P/O = 10/6.07/25.25) and 700°C (Ca/P = 1.681; Ca/P/O = 10/5.95/24.91) (Figure 5 and Table 3) are similar and in agreement with the molecular formula of HAp (Ca/P = 1.666; Ca/P/O = 10/6/26). The morphology of the samples sintered at 600°C and 700°C is similar (Figure 6).

The BET results show that the specific surface area increases slightly as the temperature increases from 600°C to 700°C (Table 2). However, the fabrication of 700°C HAp granules requires more energy; therefore, the appropriate conditions for the fabrication of HAp granules are PVA/HAp mass ratio of 3/20, a sintering temperature of 600°C, and a sintering time of 4 h. These fabricated H_3 granules are used to remove Pb^{2+} ions for further studies (Figure 7).

3.2. Effect of the Experimental Factors on Pb^{2+} Treatment Process by HAp Granules

3.2.1. Determination of pH_{PZC} of HAp Granules. The variation of ΔpH versus pH_0 (initial pH) of HAp granules is shown

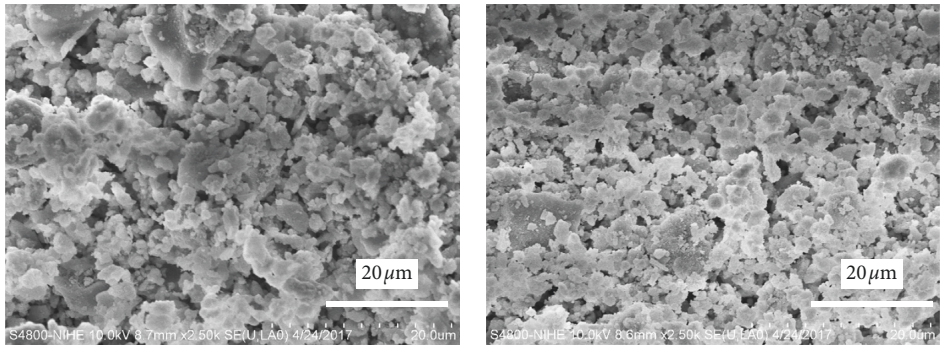

(a) (b)

Figure 3: SEM images of (a) H_2 and (b) H_3 granules sintered at 600°C for 4 h.

Table 2: The effect of sintering temperature on the color, durability in water, and specific surface area of H_3 granules.

Temperature (°C)									
400			600			700			
Color	% mass		Color	% mass		S_{BET} (m^2/g)	Color	% mass		S_{BET} (m^2/g)
	4 h	8 h		4 h	8 h			4 h	8 h	
Black	26	43	White	10	20	70.6	White	8	16.8	73.0

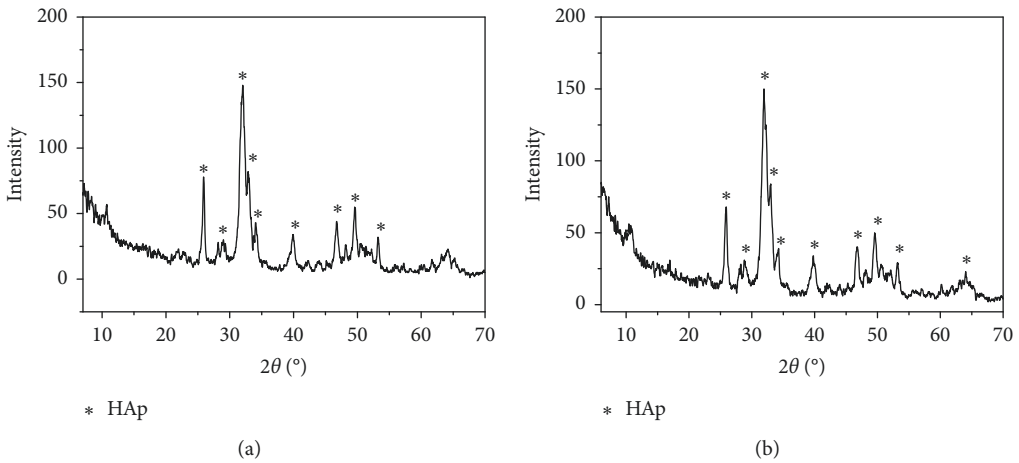

(a) (b)

Figure 4: XRD patterns of H_3 granules sintered at (a) 600°C and (b) 700°C.

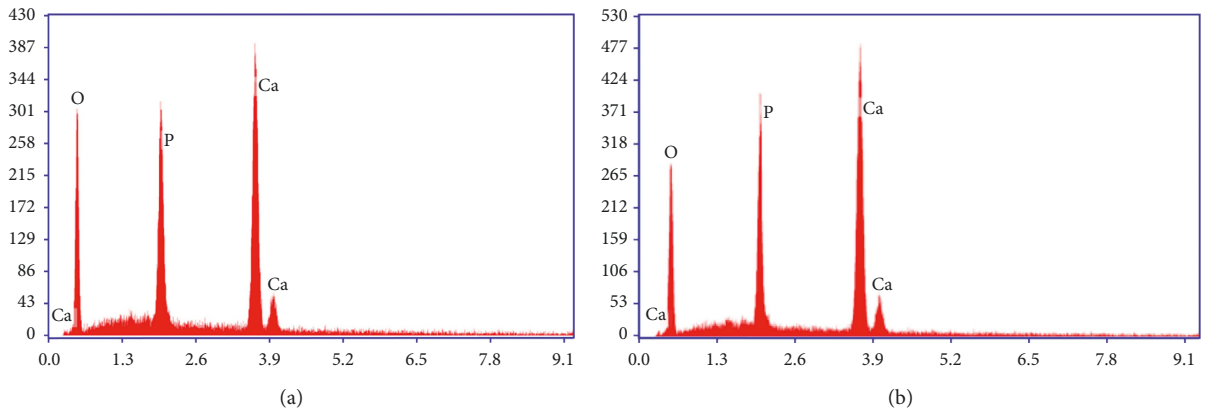

(a) (b)

Figure 5: EDX spectra of H_3 granules sintered at (a) 600°C and (b) 700°C.

Table 3: Component of elements in H_3 granules sintered at 600°C and 700°C.

T (°C)	Content (%)	Element		
		P	Ca	O
600	weight	18.98	40.31	40.71
	atom	14.71	24.21	61.08
700	weight	18.75	40.71	40.54
	atom	14.56	24.48	60.96

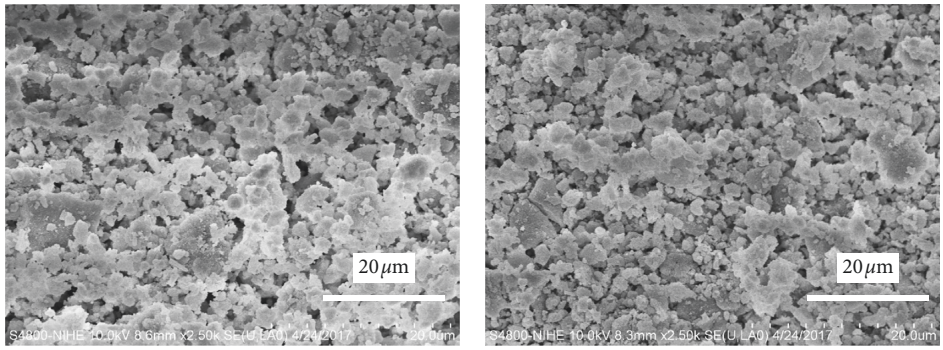

(a) (b)

Figure 6: SEM images of H_3 granules sintered at (a) 600°C and (b) 700°C.

Figure 7: Digital photo of H_3 granules prepared at 600°C for 4 h (PVA/HAp = 3/20).

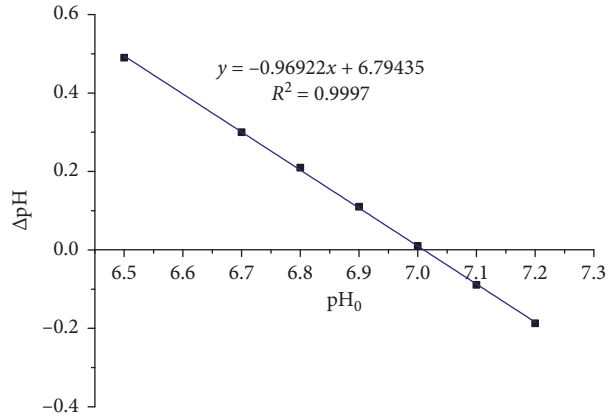

Figure 8: The variation of ΔpH versus pH_0.

in Figure 8, and it can be seen that ΔpH = 0 at $pH_0 = 7.01$. This means that the pH_{PZC} of HAp granules is 7.01.

3.2.2. Effect of Contact Time. Figure 9 shows the variation of the adsorption capacity and the removal efficiency of the HAp granules for Pb^{2+} ions as a function of the contact time. The adsorption capacity (Q, mg/g) and the removal efficiency (H, %) increase rapidly during the first 30 min and then increase slowly and reach steady state after 40 min because the adsorption process has tended to reach equilibrium. To obtain high adsorption capacity and removal efficiency, a contact time of 40 min is chosen for subsequent studies.

3.2.3. Effect of pH. The removal efficiency of Pb^{2+} strongly depends on the pH of the solution because the surface properties of the adsorbent are modified by the pH. From $pH_{PZC} = 7.01$, the experiments were investigated at a pH of about 7.01. However, by avoiding the precipitation of $Pb(OH)_2$ in an alkaline media (pH > 7.5), the effect of pH is conducted with a pH ≤ 7.5. The variation of the adsorption capacity and the removal efficiency of Pb^{2+} with the pH values is illustrated in Figure 10. In the pH range of 2.5 to 7.5, the adsorption capacity and the removal efficiency increase with increasing pH. This is because in acidic media, HAp granules are protonated and their surface is positively charged, resulting in a decrease in the amount of adsorption sites. In addition, there is an adsorption competition between H^+ and Pb^{2+} ions, which decreases the adsorption capacity and the removal efficiency of Pb^{2+}. On the contrary, at low pH, some of the HAp granules are dissolved. Therefore, pH values of 4.4 to 7.5 can be chosen. However, in order to have the advantage for the treatment process, the pH_0 5.5 is chosen for Pb^{2+} adsorption in subsequent investigations.

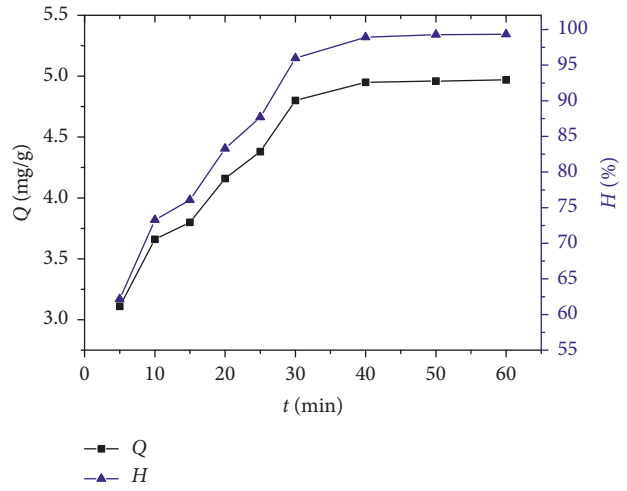

Figure 9: The variation of Pb^{2+} adsorption capacity and removal efficiency according to contact time ($m_{HAp\ granules} = 6$ g/L; $C_0 = 30$ mg/L; pH_0 5.5; $T = 30^{\circ}C$).

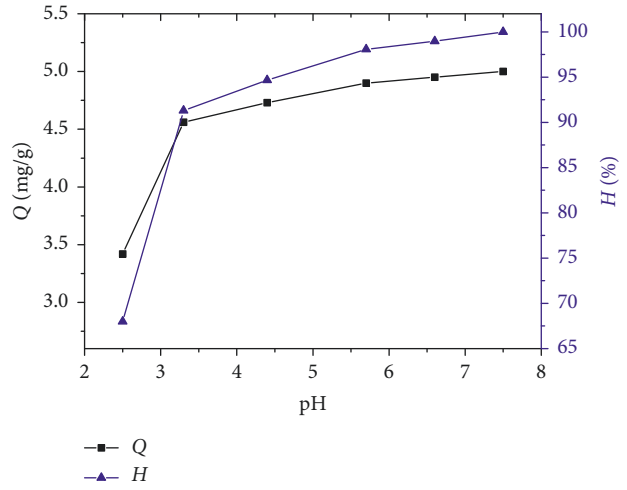

Figure 10: The effect of the pH value on the adsorption capacity and the removal efficiency of Pb^{2+} ($m_{HAp\ granules} = 6$ g/L; $C_0 = 30$ mg/L; $t_{contact} = 40$ min; $T = 30^{\circ}C$).

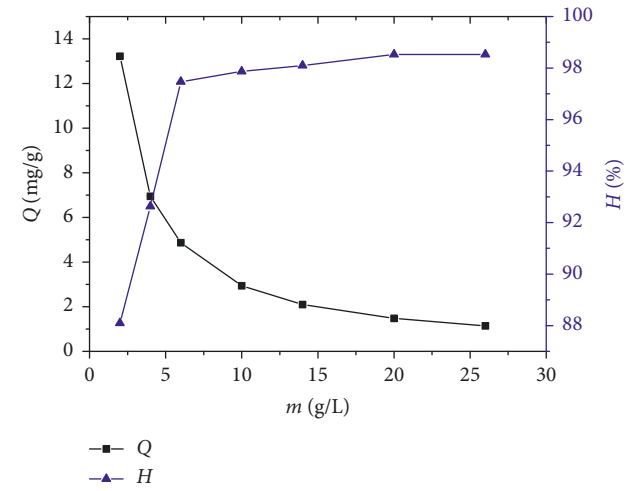

Figure 11: The effect of HAp granules mass on the adsorption capacity and the removal efficiency of Pb^{2+} ($C_0 = 30$ mg/L; pH_0 5.5; $t_{contact} = 40$ min; $T = 30^{\circ}C$).

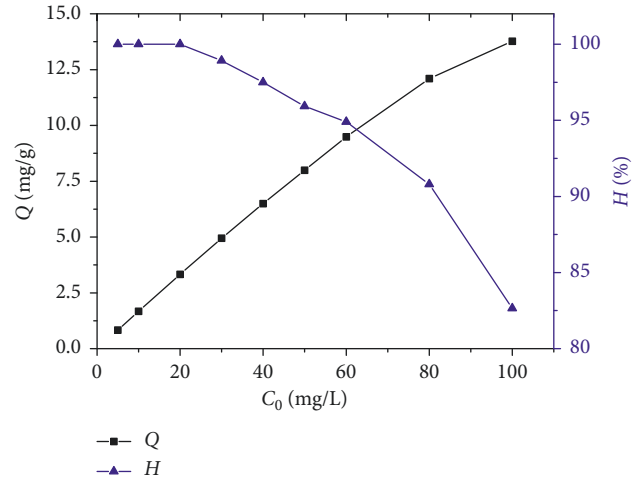

Figure 12: The effect of initial Pb^{2+} concentration on the adsorption capacity and the removal efficiency of Pb^{2+} ($m_{HAp\ granules} = 6$ g/L; pH_0 5.5; $t_{contact} = 40$ min; $T = 30^{\circ}C$).

3.2.4. Effect of Adsorbent Mass. The effect of the mass of HAp granules on the adsorption capacity and the removal efficiency of Pb^{2+} is presented in Figure 11. It can be seen that when the mass of HAp granules increases from 2 to 6 g/L, the adsorption capacity decreases from 12.33 to 4.87 mg/g and the removal efficiency increases from 88.10 to 97.47%. When the adsorbent mass varies from 6 to 20 g/L, the adsorption capacity increases slowly and reaches 98.53% at the equilibrium condition. To obtain a high combined adsorption capacity of 4.87 mg/g and removal efficiency of 97.47 %, the mass of HAp granules of 6 g/L is chosen for the removal of Pb^{2+}.

3.2.5. Effect of Initial Pb^{2+} Concentration. The initial concentration of Pb^{2+} has a significant effect on the adsorption capacity and the removal efficiency. When the concentration of Pb^{2+} is increased, the adsorption capacity increases while the removal efficiency decreases (Figure 12). To obtain a high combined adsorption capacity and removal efficiency, Pb^{2+} concentration can be used in the range of 30 – 60 mg/L. Maximum removal efficiency of 95.92% has been obtained for the initial Pb^{2+}concentration of 50 mg/L. The removal efficiency of HAp granules in this work is relatively high compared to other adsorbent materials reported in the literature [39]. Its corresponding adsorption capacity is 7.99 mg/g, lower than that of the HAp powder because the specific surface area of the HAp in the form of granules is less than that of the powder [16]. However, the HAp granules can easily be filtered from the solution and could therefore be applied under real conditions (Figure 7).

Table 4: The values of $\ln C_e$, $\ln Q$, and C_e/Q ratio determined from the different initial concentrations of Pb^{2+}.

C_0 (mg/L)	C_e (mg/L)	$\ln C_e$	Q (mg/g)	$\ln Q$	C_e/Q (g/L)
30	0.32	−1.13	4.95	1.60	0.06
40	0.97	−0.03	6.50	1.90	0.15
50	2.34	0.85	7.94	2.07	0.30
60	2.7	0.99	9.49	2.25	0.28
80	7.35	2.00	12.10	2.49	0.57
100	17.35	2.85	13.77	2.62	1.26

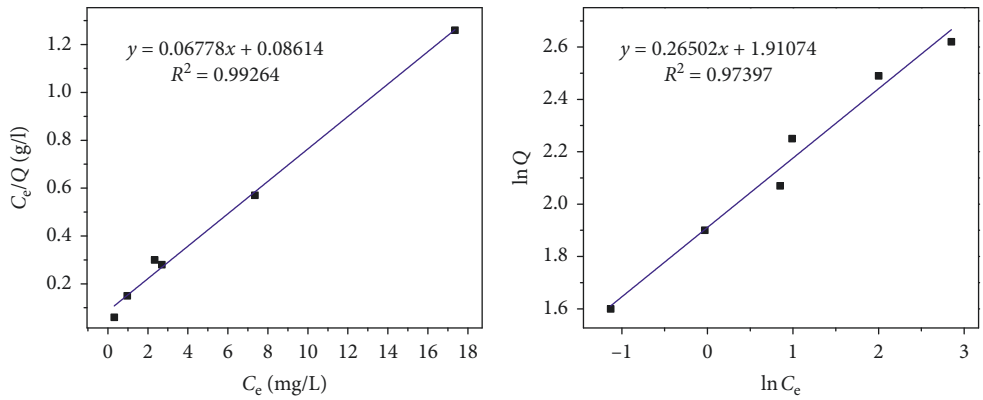

Figure 13: Adsorption isotherm curves at 30°C follow (a) Langmuir and (b) Freundlich models.

3.3. Adsorption Isotherm. The appropriate conditions for the removal of Pb^{2+} are 6 g/L HAp granule, a contact time of 40 min, a pH_0 value of 5.5, and a reaction temperature of 30°C. By varying the initial concentration of Pb^{2+} and determining the remaining Pb^{2+} concentration at equilibrium (C_e), the values of $\ln C_e$, $\ln Q$, and C_e/Q ratio can be calculated (Table 4). From this, Langmuir (Figure 13(a)) and Freundlich (Figure 13(b)) adsorption isothermal equations can be established. Accordingly, both Langmuir and Freundlich adsorption constants can be calculated, and the result is shown in Table 5.

From the results obtained, both adsorption isotherm models can describe experimental data of the adsorption of Pb^{2+} by HAp granules. However, the R^2 value of the Langmuir isotherm ($R^2 = 0.99264$) is higher than that of the Freundlich isotherm ($R^2 = 0.97397$), indicating that the Langmuir isotherm is more appropriate than the Freundlich isotherm.

3.4. Adsorption Kinetics. By varying the reaction time, the graphs of pseudo-first-order (Figure 14(a)) and pseudo-second-order (Figure 14(b)) kinetic equations are established.

From Figure 14, the adsorption rate constant (k) and the equilibrium adsorption capacity (Q_e) can be calculated. The results are presented in Table 6. Table 6 shows that the Q_e value calculated from pseudo-first-order kinetic equation (6.32 mg/g) differs from the experimentally obtained Q_e value (4.97 mg/g); in this case, the correlation coefficient $R^2 = 0.92245$ is diverging by 1. On the contrary, Q_e calculated from pseudo-second-order kinetic equation (5.43 mg/g) is very little different from the experimental Q_e (4.97 mg/g), and simultaneously, the correlation coefficient $R^2 = 0.99648$ is very close to 1. These results prove that the pseudo-second-order kinetic equation is the best fit to the experimental data. Accordingly, the adsorption rate constant is 0.03680 g/mg/min.

Table 5: Experimental constants Q_m, K_L, K_F, and n in Langmuir and Freundlich equations.

Langmuir			Freundlich		
Q_m	K_L	R^2	n	K_F	R^2
14.75	0.79	0.99264	3.77	6.70	0.97397

4. Conclusions

HAp granules were fabricated from a HAp powder precursor and polyvinyl alcohol (PVA) additive by the sintering method with an average size of 2 × 10 mm and used as an effective adsorbent to remove Pb^{2+} in aqueous solution. The adsorption process depends on the pH, the adsorbent mass, the initial Pb^{2+} concentration, and contact time. Under the conditions studied, the adsorption of Pb^{2+} on HAp granules occurs rapidly and reaches equilibrium after 40 min. The adsorption process of Pb^{2+} follows the pseudo-second-order adsorption kinetic equation and the Langmuir adsorption isotherm model. The obtained results will open a direction of potential application in the adsorption column with the

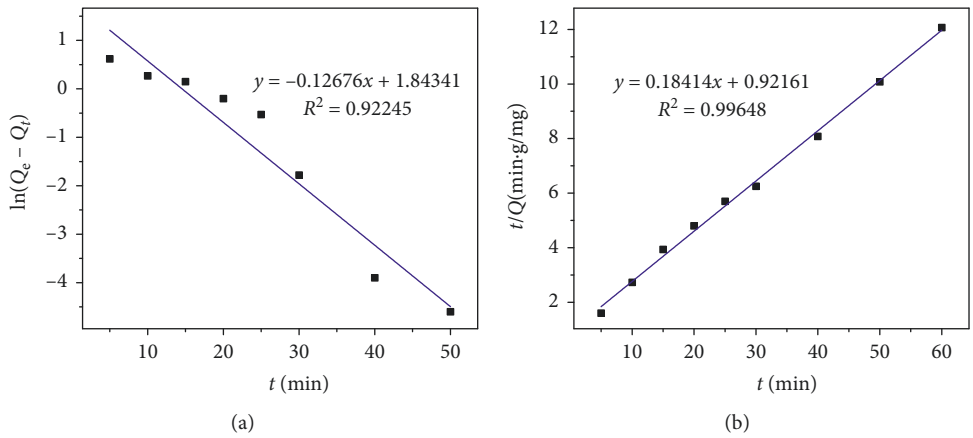

Figure 14: The description of the experimental data by (a) pseudo-first-order and (b) pseudo-second-order kinetic equations.

Table 6: The values of k and Q_e calculated from pseudo-first-order and pseudo-second-order kinetic equations.

Pseudo-first-order kinetic equation			Pseudo-second-order kinetic equation			Experimental Q_e (mg/g)
Q_e (mg/g)	k_1 (min^{-1})	R^2	Q_e (mg/g)	k_2 (g/mg/min)	R^2	
6.32	0.12676	0.92245	5.43	0.03680	0.99648	4.97

HAp granule adsorbent for the treatment of Pb^{2+} in polluted water.

Data Availability

The data used to support the findings of this study are included within the article.

Conflicts of Interest

The authors declare that there are no conflicts of interest regarding the publication of this paper.

Acknowledgments

The authors would like to thank the financial support of project of Ministry of Education and Training (code: B2017-15ĐT) for completing this work.

References

[1] F. Fu and Q. Wang, "Removal of heavy metal ions from wastewaters: a review," *Journal of Environmental Management*, vol. 92, no. 3, pp. 407–418, 2011.

[2] R. A. Wuana and F. E. Okieimen, "Heavy metals in contaminated soils: a review of sources, chemistry, risks and best available strategies for remediation," *ISRN Ecology*, vol. 2011, Article ID 402647, 20 pages, 2011.

[3] L. Li, X. Dong, Y. Dong, L. Zhu, S. J. You, and Y. F. Wang, "Incorporation of zinc for fabrication of low-cost spinel-based composite ceramic membrane support to achieve its stabilization," *Journal of Hazardous Materials*, vol. 287, pp. 188–196, 2015.

[4] W. Y. Xia, Y. S. Feng, F. Jin, L. M. Zhang, and Y. J. Du, "Stabilization and solidification of a heavy metal contaminated site soil using a hydroxyapatite based binder," *Construction and Building Materials*, vol. 156, pp. 199–207, 2017.

[5] K. Shih, T. White, and J. O. Leckie, "Spinel formation for stabilizing simulated nickel-laden sludge with aluminum-rich ceramic precursors," *Environmental Science and Technology*, vol. 40, no. 16, pp. 5077–5083, 2006.

[6] L. Li, X. Dong, Y. Dong, Y. M. Zheng, L. Zhu, and J. Liu, "Thermal conversion of hazardous metal copper via the preparation of $CuAl_2O_4$ spinel-based ceramic membrane for potential stabilization of simulated copper-rich waste," *ACS Sustainable Chemistry and Engineering*, vol. 3, no. 11, pp. 2611–2618, 2015.

[7] M. Ziagova, G. Dimitriadis, D. Aslanidou, X. Papaioannou, E. Litopoulou Tzannetaki, and M. Liakopoulou-Kyriakides, "Comparative study of Cd(II) and Cr(VI) biosorption on *Staphylococcus xylosus* and *Pseudomonas* sp. in single and binary mixtures," *Bioresource Technology*, vol. 98, no. 15, pp. 2859–2865, 2007.

[8] S. Shanmugam and B. Gopal, "Copper substituted hydroxyapatite and fluorapatite: synthesis, characterization and antimicrobial properties," *Ceramics International*, vol. 40, no. 10, pp. 15655–15662, 2014.

[9] E. A. Krylova, S. E. Krylov, I. G. Plashchina, and P. V. Nefedov, "Hydroxyapatite-alginate structure as living cells supporting system," *Minerva Biotecnologica*, vol. 18, no. 1, pp. 17–22, 2006.

[10] A. Kasioptas, C. Perdikouri, C. V. Putnis, and A. Putnis, "Pseudomorphic replacement of single calcium carbonate crystals by polycrystalline apatite," *Mineralogical Magazine*, vol. 72, no. 1, pp. 77–80, 2008.

[11] V. C. Tim, "Porous scaffolds for the replacement of large bone defects: a biomechanical design study," Ph.D. thesis, Katholieke Universiteit Leuven, Leuven, Belgium, 2005.

[12] A. Corami, S. Mignardi, and V. Ferrini, "Cadmium removal from single- and multi-metal () solutions by sorption on hydroxyapatite," *Journal of Colloid and Interface Science*, vol. 317, no. 2, pp. 402–408, 2008.

[13] G. Neha, A. K. Kushwaha, and M. C. Chattopadhyaya, "Adsorption studies of cationic dyes onto Ashoka (*Saraca*

asoca) leaf powder," *Journal of the Taiwan Institute of Chemical Engineers*, vol. 43, no. 4, pp. 604–613, 2012.

[14] I. Mobasherpour, E. Salahi, and M. Pazouki, "Comparative of the removal of Pb^{2+}, Cd^{2+} and Ni^{2+} by nano crystallite hydroxyapatite from aqueous solutions: adsorption isotherm study," *Arabian Journal of Chemistry*, vol. 5, no. 4, pp. 439–446, 2012.

[15] M. S. Fernando, R. M. de Silva, and K. M. N. de Silva, "Synthesis, characterization, and application of nano hydroxyapatite and nanocomposite of hydroxyapatite with granular activated carbon for the removal of Pb2+ from aqueous solutions," *Applied Surface Science*, vol. 351, pp. 95–103, 2015.

[16] S. M. Mousa, N. S. Ammar, and H. A. Ibrahim, "Removal of lead ions using hydroxyapatite nano-material prepared from phosphogypsum waste," *Journal of Saudi Chemical Society*, vol. 20, no. 3, pp. 357–365, 2016.

[17] N. P. Raval, P. U. Shah, and N. K. Shah, "Adsorptive removal of nickel(II) ions from aqueous environment: a review," *Journal of Environmental Management*, vol. 179, pp. 1–20, 2016.

[18] Y. Li, D. Wang, and S. Lim, "Fabrication and applications of metal-ion-doped hydroxyapatite nanoparticles," *Juniper Online Journal Material Science*, vol. 1, no. 2, article 555558, 2017.

[19] M. Islam, P. Chandra Mishra, and R. Patel, "Physicochemical characterization of hydroxyapatite and its application towards removal of nitrate from water," *Journal of Environmental Management*, vol. 91, no. 9, pp. 1883–1891, 2010.

[20] W. Wei, R. Sun, J. Cui, and Z. Wei, "Removal of nitrobenzene from aqueous solution by adsorption on nanocrystalline hydroxyapatite," *Desalination*, vol. 263, no. 1–3, pp. 89–96, 2010.

[21] D. Zhang, H. Luo, L. Zheng et al., "Utilization of waste phosphogypsum to prepare hydroxyapatite nanoparticles and its application towards removal of fluoride from aqueous solution," *Journal of Hazardous Materials*, vol. 241-242, pp. 418–426, 2012.

[22] A. Bahdod, S. El Asri, A. Saoiabi, T. Coradin, and A. Laghzizil, "Adsorption of phenol from an aqueous solution by selected apatite adsorbents: kinetic process and impact of the surface properties," *Water Research*, vol. 43, no. 2, pp. 313–318, 2009.

[23] H. Hou, R. Zhou, P. Wu, and L. Wu, "Removal of Congo red dye from aqueous solution with hydroxyapatite/chitosan composite," *Chemical Engineering Journal*, vol. 211-212, pp. 336–342, 2012.

[24] S. Hokkanen, E. Repo, L. J. Westholm, S. Lou, T. Sainio, and M. Sillanpää, "Adsorption of Ni^{2+}, Cd^{2+}, $PO4^{3-}$ and NO^{3-} from aqueous solutions by nanostructured microfibrillated cellulose modified with carbonated hydroxyapatite," *Chemical Engineering Journal*, vol. 252, pp. 64–74, 2014.

[25] K. Kandori, M. Oketani, and M. Wakamura, "Effects of Ti(IV) substitution on protein adsorption behaviors of calcium hydroxyapatite particles," *Colloids and Surfaces B: Biointerfaces*, vol. 101, pp. 68–73, 2013.

[26] K. H. Zuo, Y. P. Zeng, and D. Jiang, "Effect of polyvinyl alcohol additive on the pore structure and morphology of the freeze-cast hydroxyapatite ceramics," *Materials Science and Engineering: C*, vol. 30, no. 2, pp. 283–287, 2010.

[27] D. J. Veljović, I. Zalite, E. Palcevskis, I. Smiciklas, R. Petrović, and D. J. Janaćković, "Microwave sintering of fine grained HAP and HAP/TCP bioceramics," *Ceramics International*, vol. 36, no. 2, pp. 595–603, 2010.

[28] D. M. Liu, "Preparation and characterisation of porous hydroxyapatite bioceramic via a slip-casting route," *Ceramics International*, vol. 24, no. 6, pp. 441–446, 1998.

[29] K. Zhao, Y. F. Tang, Y. S. Qin, and J. Q. Wei, "Porous hydroxyapatite ceramics by ice templating: freezing characteristics and mechanical properties," *Ceramics International*, vol. 37, no. 2, pp. 635–639, 2011.

[30] J. Locs, V. Zalite, L. Berzina-Cimdina, and M. Sokolova, "Ammonium hydrogen carbonate provided viscous slurry foaming-A novel technology for the preparation of porous ceramics," *Journal of the European Ceramic Society*, vol. 33, no. 15-16, pp. 3437–3443, 2013.

[31] I. Sopyan and J. Kaur, "Preparation and characterization of porous hydroxyapatite through polymeric sponge method," *Ceramics International*, vol. 35, no. 8, pp. 3161–3168, 2009.

[32] I. Sopyan, M. Mel, S. Ramesh, and K. A. Khalid, "Porous hydroxyapatite for artificial bone applications," *Science and Technology of Advanced Materials*, vol. 8, no. 1-2, pp. 116–123, 2007.

[33] W. Suchanek and M. Yoshimura, "Processing and properties of hydroxyapatite-based biomaterials for use as hard tissue replacement implants," *Journal of Materials Research*, vol. 13, no. 1, pp. 94–117, 1998.

[34] C. M. Simonescu, A. Melinescu, I. Melinte, R. Elena-Patescu, and M. Dragne, "Copper removal from synthetic aqueous solutions by hydroxyapatite granules synthesized using microwave heating," in *Proceedings of SGEM 2015 Conference*, vol. 1, pp. 177–184, Albena, Bulgaria, June 2015, ISBN 978-619-7105-39-1/ISSN-1314-2704.

[35] T. M. Hieu Do, P. T. T. Tran, A. K. Ton, and M. V. Le, "A novel method for the fabrication of granular hydroxyapatite-bentonite composite adsorbents for the removal of Pb^{2+} from an aqueous solution," *Journal of Environmental Science and Engineering B*, vol. 5, no. 7, pp. 371–378, 2016.

[36] T. T. T. Pham, T. P. Nguyen, T. N. Pham et al., "Impact of physical and chemical parameters on the hydroxyapatite nanopowder synthesized by chemical precipitation method," *Advances in Natural Sciences: Nanoscience and Nanotechnology*, vol. 4, no. 3, article 035014, 2013.

[37] I. Smičiklas, A. Onjia, and S. Raičević, "Experimental design approach in the synthesis of hydroxyapatite by neutralization method," *Separation and Purification Technology*, vol. 44, no. 2, pp. 97–102, 2005.

[38] T. Mohammadreza, S. H. Mehran, and E. Hossein, "Synthesis and characterization of hydroxyapatite nanocrystals via chemical precipitation technique," *Iranian Journal of Pharmaceutical Sciences*, vol. 4, no. 2, pp. 127–134, 2008.

[39] J. M. Rivera, S. Rincón, C. B. Youssef, and A. Zepeda, "Highly efficient adsorption of aqueous Pb(II) with mesoporous metal-organic framework-5: an equilibrium and kinetic study," *Journal of Nanomaterials*, vol. 2016, Article ID 8095737, 9 pages, 2016.